1986ApJ...306..740H

THE ASTROPHYSICAL JOURNAL, 306:740–750, 1986 July 15
© 1986. The American Astronomical Society. All rights reserved. Printed in U.S.A.

SOLAR CORONAL BRIGHT POINTS OBSERVED WITH THE VLA

SHADIA R. HABBAL, ROBERT S. RONAN, AND GEORGE L. WITHBROE
Harvard-Smithsonian Center for Astrophysics
AND
RAGHUNATH K. SHEVGAONKAR[2] AND MUKUL R. KUNDU
Astronomy Program, University of Maryland
Received 1985 October 25; accepted 1986 January 9

ABSTRACT

We report on the first observations of solar coronal bright points made at 20 cm wavelength with the VLA. The brightness temperature of the sources observed varies between 1 and 5×10^5 K. The observations indicate that significant fluctuations in the brightness temperature as well as in the spatial extent of these sources can occur over a few minutes, These fluctuations are shown to be due to density and temperature fluctuations at transition region heights combined with either plasma motions along magnetic field lines or changes in magnetic field topology, or both.

Subject headings: Sun: corona — Sun: radio radiation

I. INTRODUCTION

First identified in XUV and X-ray spectroheliograms (e.g., Golub *et al.* 1974), coronal bright points appear to be collections of miniature loops or arches, typically 10″–20″ in length. Sheeley and Golub (1979) found that the emission from bright points changes significantly over a few minutes. A detailed study of EUV data from *Skylab* (Habbal and Withbroe 1981) showed that, over a period of 5 minutes—the shortest time scale available from the data—strong temporal and spatial variations in intensity of emission occur in the chromospheric through coronal layers of the bright points. Habbal and Withbroe (1981) attributed the changes in EUV emission to intermittent heating, possibly correlated with changes in magnetic field topologies over very small scales (a few arc seconds or less). More recently, Harvey (1985) has shown that features which appear as "dark" absorption regions in the He I λ10830 line and are believed to be the photospheric counterpart of coronal bright points are often associated with encounters of existing opposite polarity magnetic regions rather than emerging magnetic flux. In λ10830 they are also observed to be short lived (on the order of hours), often appearing and disappearing over a few minutes.

Attempts to detect coronal bright points at radio wavelengths have been scarce, mainly because of the constraints of both spatial and temporal resolution (Marsh and Hurford 1982). The association of type III bursts with flaring X-ray bright points was made by Kundu, Gergely, and Golub (1980); the number of events, however, was limited to four in a period of 430 hr of observations during part of the *Skylab* period. In a map of a quiet-Sun field at 4.9 GHz made with the VLA, Marsh, Hurford, and Zirin (1980) found bright features to coincide with small bipolar regions but not with the chromospheric network. They suggested that X-ray bright points provide a significant fraction of the quiet-Sun radio signal. In this paper we present the results of an attempt to detect coronal bright points at radio wavelengths using the VLA. We show that the 20 cm wavelength radio emission from bright points arises mainly from heights typical of the low corona-transition region and exhibits the same spatial and temporal variability observed earlier at X-ray, EUV, and optical wavelengths. The fluctuations in radio emission are shown to be most likely due to intermittent heating where the magnetic field could be playing an important role.

II. OBSERVATIONS

Solar radio observations were acquired on 1984 February 11 using the VLA in the B-configuration. The field of view was centered at $-25°$ south and $+36°$ west at 18:00 UT; this coincided with a coronal hole on the disk which was determined from a He λ10830 map of the disk (courtesy J. Harvey). The observations at $\lambda = 20$ cm were made for a total of 2 hr with a 1 hr data gap when observations at $\lambda = 6$ cm were made. There were also short (minutes) data gaps coinciding with the pointing of the antennas to the calibration source. The receiver bandwidth selected was 12.5 MHz. For observations at 20 cm the best spatial resolution for the VLA in the B-configuration is 4″.

Several bright radio sources were first detected by making an integrated map of the field of view ($\sim$30′) using data from the entire 2 hr of measurements at $\lambda = 20$ cm. Since our aim was to detect changes in emission over minutes, we then made 20, 2 minute integrated maps for the first observing hour. Some sources prominent in the 2 minute maps were absent from the 2 hr integrated map where time-averaging reduced sources lasting less than several hours to the noise level. Care was taken to eliminate spurious sources caused by sidelobe effects; in particular, sources that rotated in time with the synthesized beam. Using the antenna beam pattern, we also made sure that no real source coincided with a sidelobe of another source. Although this procedure may have eliminated some short-lived (<a few minutes) sources, no other method appeared to provide enough confidence about the reality of the detected sources which were present for at least one-half hour. Once the sources were determined, the 20, 2 minute maps were

[1] The VLA is a facility of the National Radio Astronomy Observatory, which is operated by Associated Universities, Inc., under contract with the National Science Foundation.

[2] Permanent Address: Indian Institute of Astrophysics, Bangalore, India.

© American Astronomical Society • Provided by the NASA Astrophysics Data System

1986ApJ...306..740H

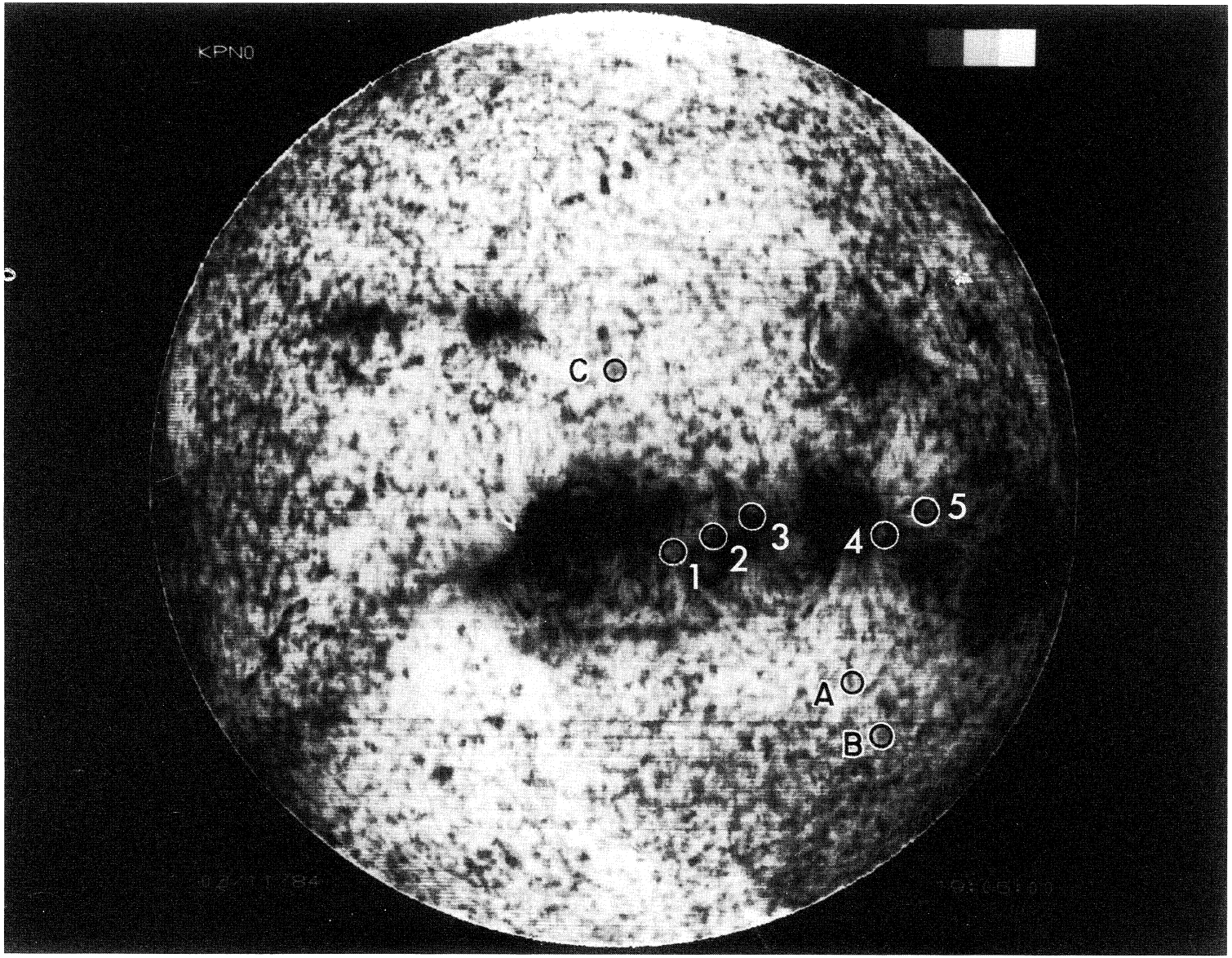

FIG. 1*a*

FIG. 1.—Solar coronal radio sources observed on 1984 February 11 with the VLA at $\lambda = 20$ cm, superposed on (*a*) a Kitt Peak He I λ10830 spectroheliogram made at 15:12 UT and (*b*) a magnetogram made at 19:06 UT. (Both courtesy J. Harvey). Sources labeled 1–5 coincide with active regions, those labeled A, B, and C are in the quiet Sun and are the coronal bright points studied in this paper.

© American Astronomical Society • Provided by the NASA Astrophysics Data System

1986ApJ...306..740H

© American Astronomical Society • Provided by the NASA Astrophysics Data System

1986ApJ...306..740H

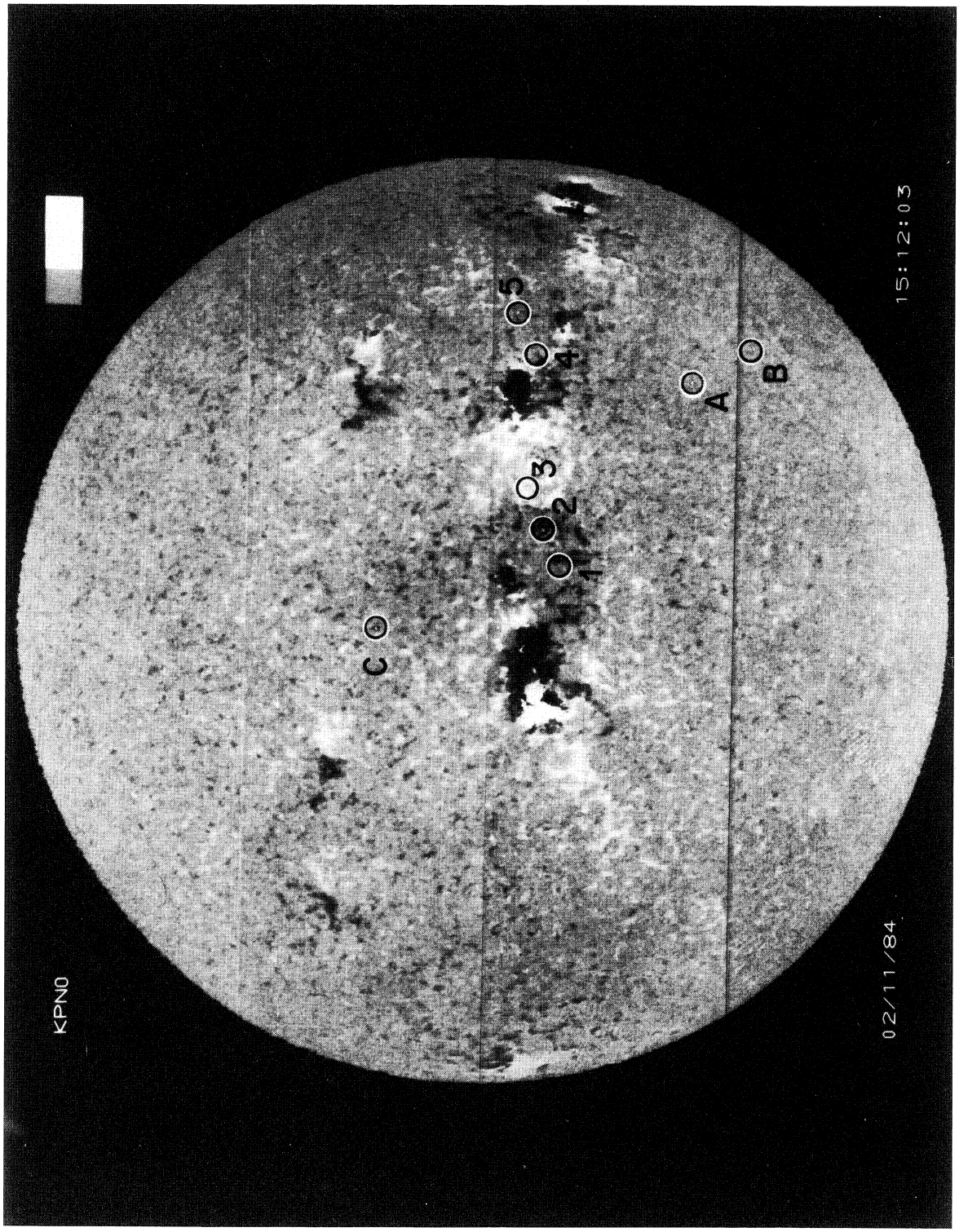

FIG. 1b

© American Astronomical Society • Provided by the NASA Astrophysics Data System

1986ApJ...306..740H

© American Astronomical Society • Provided by the NASA Astrophysics Data System

1986ApJ...306..740H

CLEANed using the procedure developed by Clark (1980) with a beamwidth of 15″.

We also compared our sources with a Kitt Peak He λ10830 spectroheliogram (acquired at 19:06 UT) and a full-disk magnetogram (acquired at 15:25 UT) (courtesy J. Harvey). These are shown in Figures 1*a* and 1*b*, respectively, with the bright radio sources (acquired between 18:00 and 20:00 UT) superimposed on them. Among the radio sources found five (labeled 1–5 in Fig. 1) were located around the solar equator in an active region, while the other three (A, B, and C) were in quiet regions. None were in the "coronal hole." Sources A, B, and C seem to be likely candidates for bright points as they coincide with dark He λ10830 points, although not with conspicuous ones (see Fig. 1*a*). However, there are many more He dark points with no radio counterparts at 20 cm wavelength. In fact, the radio sources detected might only correspond to the strongest ones, the presence of many more weaker bright points could be masked by the quiet-Sun emission at this wavelength. The magnetogram (Fig. 1*b*) shows no indication of exceptionally strong bipolar features underlying the radio bright points. Since the magnetogram represents an average field and was made ~3 hr earlier than the data analyzed, it does not necessarily provide the appropriate measure for rapidly changing features. However, for more slowly varying features it is an appropriate measure.

The total brightness temperature contours of the CLEANed maps for sources A and B are shown in Figure 2, and source C is shown in Figure 3. (Since source C disappeared after 18:51, only 19 panels appear in Fig. 3). The contours are equally spaced starting at the 2.5 σ level of 5×10^4 K. Our 2.5 σ level falls in the range of quoted quiet-Sun brightness temperatures ranging from 5×10^4 K (Dulk 1985; Kundu 1965) to 10^5 K (Dulk and Gary 1983). The data gap occurring almost midway along the sequence (between 18:24 and 18:35 UT) coincides with the pointing of the antennas to the calibration source. The tick marks around each panel are at intervals of 40″ in Figure 2, and in Figure 3 at intervals of 40″ in the vertical direction and 20″ in the horizontal. These marks make the spatial changes occurring in the sources easier to follow in time. The spatial extent of the sources shown in Figures 2 and 3 is 40″ or less, a size typical of coronal bright points observed at EUV wavelengths but 2–3 times greater than those observed in the X-ray. It is clear from these figures that significant changes in the brightness temperature can occur over 2 minutes or longer. Significant spatial changes (i.e., greater than the beam size of 15″) can also occur. Another interesting feature is a split that occurs in some sources where one part disappears while another grows and decays in time (see, for example, Fig. 2, source B, between 18:04 and 18:06; or Fig. 3, source C between 18:08 and 18:10). Also, the change in size of the radio bright points is sometimes associated with an enhancement of emission, such as in source C between 18:20 and 18:37 or 18:39 and 18:41.

To follow the temporal changes in brightness temperature of sources A, B, and C more quantitatively, we show, in Figures 4, 5, and 6, the change in time of their maximum total brightness temperature (labeled *I*), the maximum brightness temperature of the right circularly polarized wave (*R*), and the brightness temperature of the left circularly polarized wave (*L*) at the location where *R* is maximum. The largest of *R* and *L* represents the brightness temperature, T_x, of the extraordinary mode, while the smallest represents the brightness temperature, T_o, of the ordinary mode, depending on the direction of the magnetic field. The total brightness temperature shown in these figures (as well as in Figs. 2 and 3) represents the average brightness temperature of the right and left circularly polarized waves, i.e.,

$$I = \tfrac{1}{2}(R + L). \tag{1}$$

Also shown in these figures is the absolute value of the degree of circular polarization, defined as

$$p = \frac{|R - L|}{R + L}. \tag{2}$$

The degree of circular polarization is significant when greater than 0.15 and is an indication of the magnetic field strength as well as the emission process (as will be discussed later).

Worth noting are the small differences in the intensities of the *R* and *L* waves and the correlation in the temporal variation of *R* and *L* with *I*. Changes in the location of the maximum intensity of emission are often correlated with a switch in maximum between *R* and *L* (compare, for example, the changes in the location of the maximum emission in Fig. 2, source A at 18:22 and 18:35, with the corresponding switch between *R* and *L* in Fig. 4; similarly for Figs. 2 and 5, source B at 18:45 and 18:47; and Figs. 3 and 6, source C at 18:02 and 18:10). This switch indicates an enhancement of emission in a region where the magnetic field is antiparallel to the line of sight over the emission from the region where the magnetic field is parallel to the line of sight. This is also a signature of a bipolar structure in the bright points; however, since we do not have simultaneous high spatial resolution magnetograms it is not possible, at this stage, to infer any additional information regarding changes in magnetic field topology.

III. ANALYSIS

To identify the plasma parameters or physical processes responsible for the observed variations of the brightness temperature we note that the brightness temperature of the extraordinary (T_{obs_x}) and ordinary (T_{obs_o}) wave modes is defined as (Zheleznyakov 1970)

$$T_{\mathrm{obs}_{x,o}} = \int_0^{\tau_L} T_e(l) e^{-\tau_{x,o}} d\tau_{x,o}: \tag{3}$$

$\tau_{x,o}$ in the integral is the optical depth, for each wave mode, respectively, from the altitude *l* until escape from the corona. The integration limits are τ_L, the optical depth along the ray to the reflection point ($\tau_{x,o} = 0$), where the observed radio frequency ω equals the plasma frequency, $\omega_L = 5.64 \times 10^4 N^{1/2}$. We will assume for now that the optical depth is dominated by the absorption due to collisions; thus, in the quasi-longitudinal approximation (i.e., for $\alpha \neq 90°$, where α is the angle between the magnetic field direction and the line of sight), it can be written as (Zheleznyakov 1970)

$$\tau_{x,o} \approx \frac{7}{\omega^2[1 \mp (\omega_B/\omega)|\cos\alpha|]^2} \int_l^\infty N_e^2 T_e^{-3/2} dl, \tag{4}$$

where *dl* is an element of path length along the line of sight, ω_B is the gyrofrequency $= eB/mc = 1.76 \times 10^7 B$ (in Gauss) in radians. The quantity N_e is the electron density in cm^{-3}, and T_e is the electron temperature in K along the line of sight. Since the observed emission, T_{obs}, ranges from 5×10^4 K to 5×10^5 K, it is most likely dominated by emission from the transition region where the temperature and density gradients are steep.

© American Astronomical Society • Provided by the NASA Astrophysics Data System

1986ApJ...306..740H

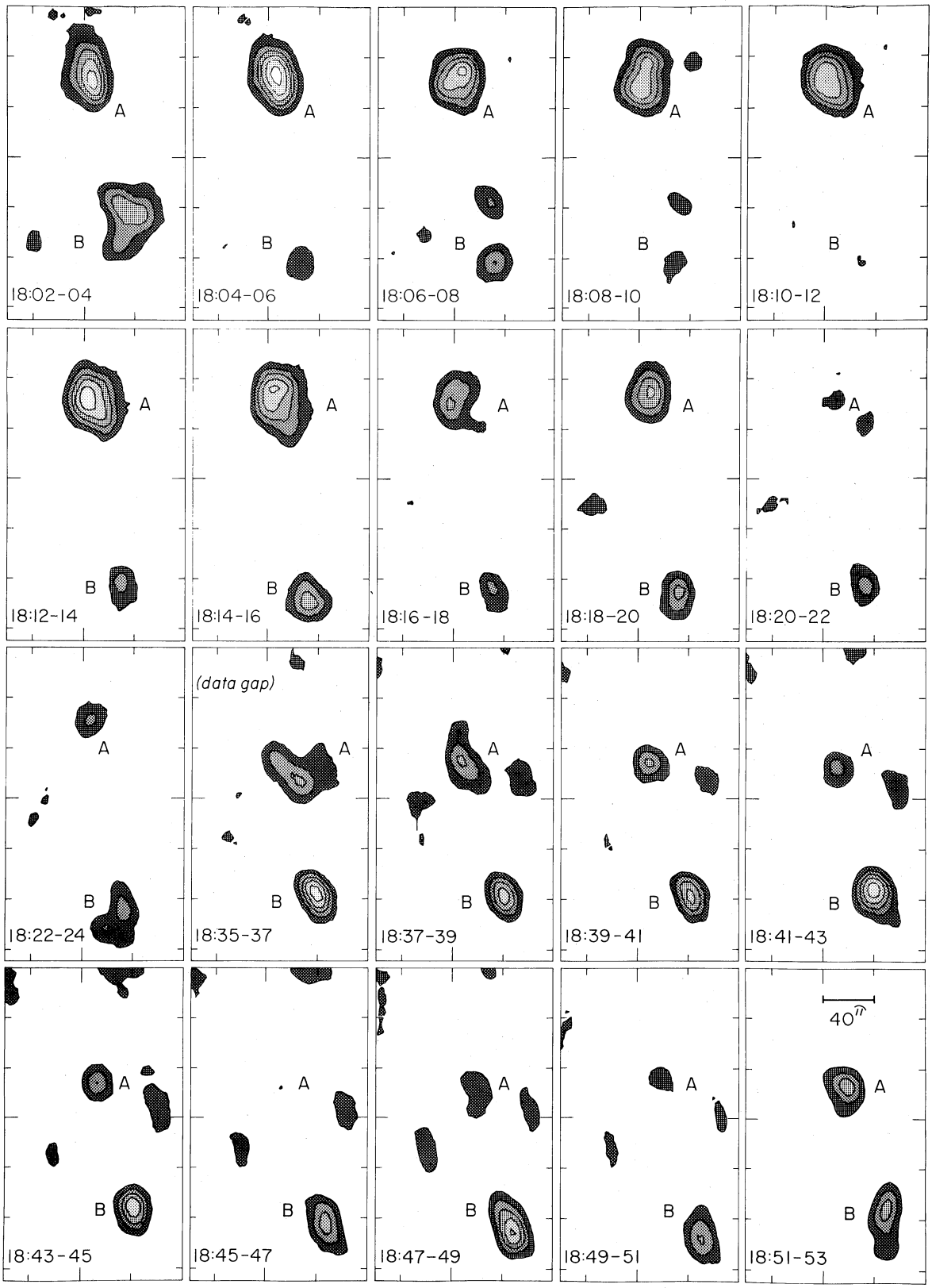

FIG. 2.—Sequence of CLEANed intensity contour maps, at $\lambda = 20$ cm, of bright points A and B. The integration time in each panel is 2 minutes. Contour levels are multiples of 5×10^4 K, the 2.5 σ level. The data gap coincides with the antennas pointing to the calibration source.

© American Astronomical Society • Provided by the NASA Astrophysics Data System

1986ApJ...306..740H

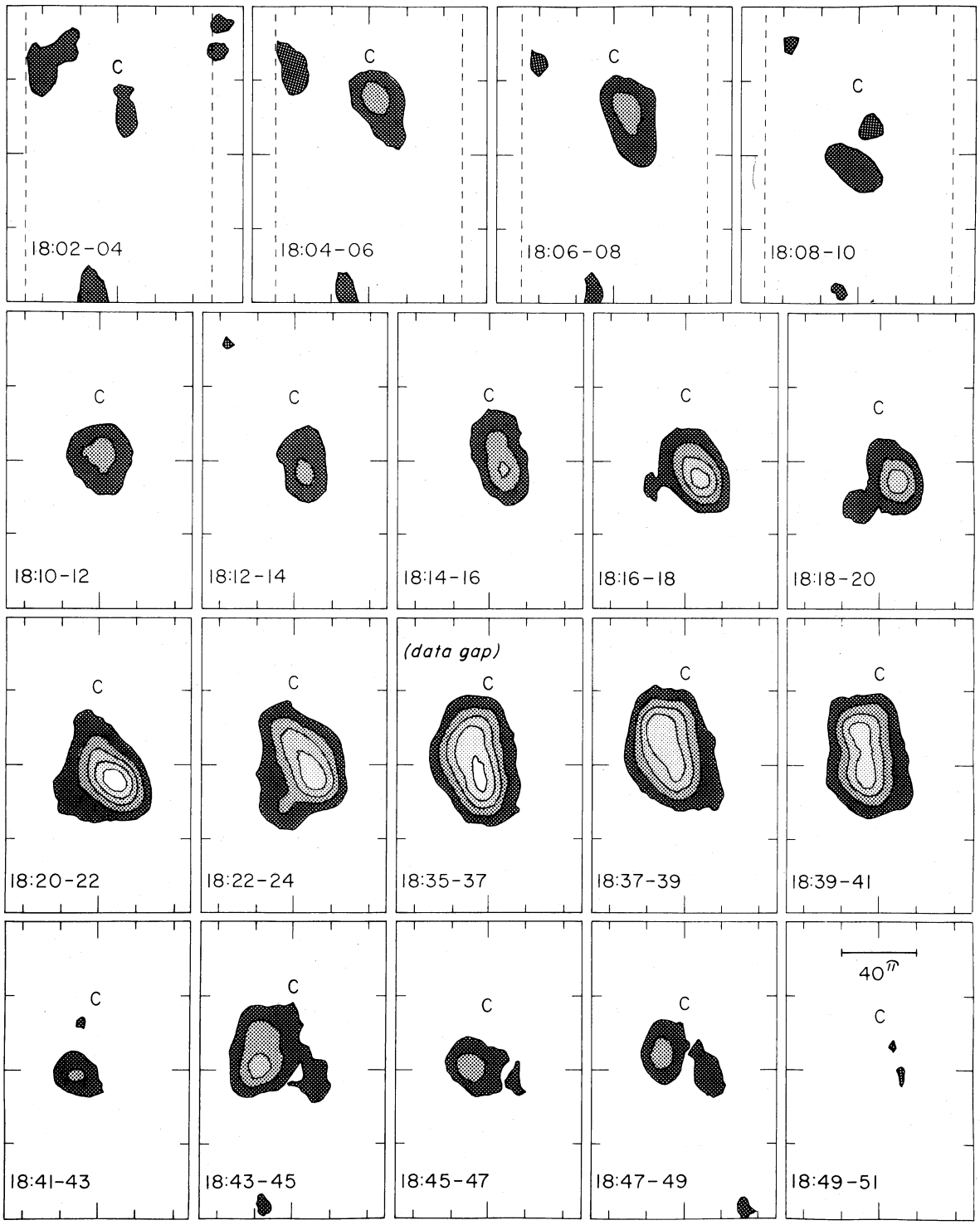

FIG. 3.—Same as Fig. 2 for bright point C

© American Astronomical Society • Provided by the NASA Astrophysics Data System

1986ApJ...306..740H

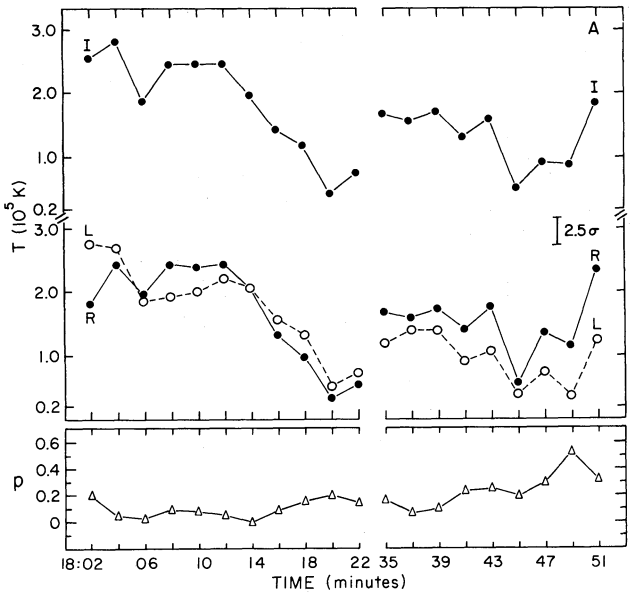

FIG. 4.—Plot of the changes in time of the total brightness temperature (*I*), the brightness temperature of the right circularly polarized wave (*R*) (*filled circles*), the left circularly polarized wave (*L*; *open circles*, *dashed line*) and the absolute value of the degree of circular polarization (*p*; *open triangle*) for bright point A. The data gap occurs between 18:22 and 18:35 UT.

We thus integrate equation (4) assuming that the scaled gas pressure, defined as

$$P_0 = N_e T_e, \tag{5a}$$

and the conductive flux,

$$F_c = 1.1 \times 10^{-6} T_e^{5/2} \frac{dT_e}{dl}, \tag{5b}$$

in the transition region, are both constant (Withbroe and Noyes 1977). Making use of equations (5a) and (5b) we substitute the integral over dl in equation (4) by an integral over dT_e and get

$$\tau_{x,o}(T) \approx \frac{7.7 \times 10^{-6}}{\omega^2[1 \mp (\omega_B/\omega)|\cos\alpha|]^2} \frac{P_o^2}{F_c} \int_T^{T_{\max}} \frac{dT_e}{T_e} \tag{6}$$

or

$$\tau_{x,o} = \log\left(\frac{T_{\max}}{T}\right)^{a_{x,o}}, \tag{7}$$

where, for simplicity, we define

$$a_{x,o} = \frac{7.7 \times 10^{-6}}{\omega^2[1 \mp (\omega_B/\omega)|\cos\alpha|]^2} \frac{P_0^2}{F_c}. \tag{8}$$

In equation (6), $T_{\max}$ is the coronal temperature and is a free parameter. Substituting the integral over $\tau_{x,o}$ in equation (4) by an integral over dT_e, with $d\tau_{x,o} = -a_{x,o}\, dT_e/T_e$ from equation (7), and the integration limits from $T_{\max}$ to T_L (the temperature at which $\omega = \omega_L$), we get

$$T_{\mathrm{obs}_{x,o}} = \frac{a_{x,o}}{a_{x,o}+1}\left[T_{\max} - \left(\frac{T_L}{T_{\max}}\right)^{a_{x,0}} T_L\right]. \tag{9}$$

Since for $\lambda = 20$ cm, the critical density, for which $\omega = \omega_L$, is $N_L = 2.8 \times 10^{10}$ cm^{-3}, $T_L < 10^5$ K for a pressure $N_L T_L$ of the order of 10^{15} cm^{-3} K, and the term $T_L/T_{\max}$ in equation (9) can be neglected. We end up with the very simple and useful relation

$$T_{\mathrm{obs}_{x,o}} = \frac{a_{x,o}}{a_{x,o}+1} T_{\max}. \tag{10}$$

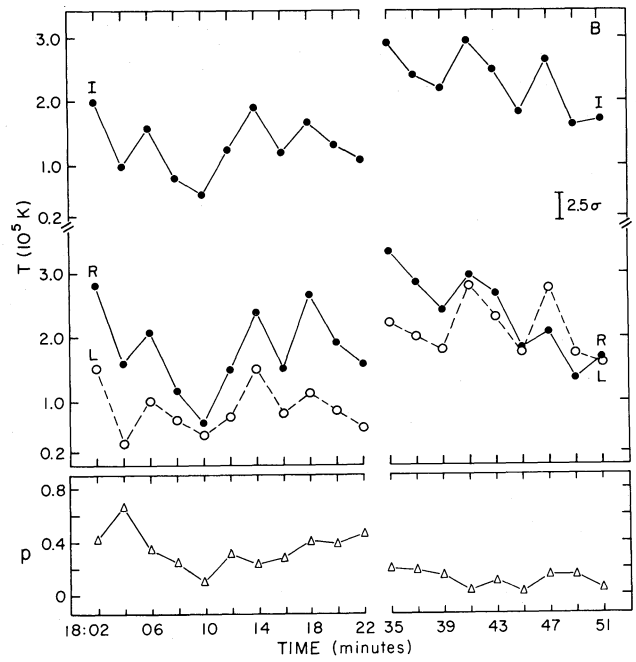

FIG. 5.—Same as Fig. 4 for source B

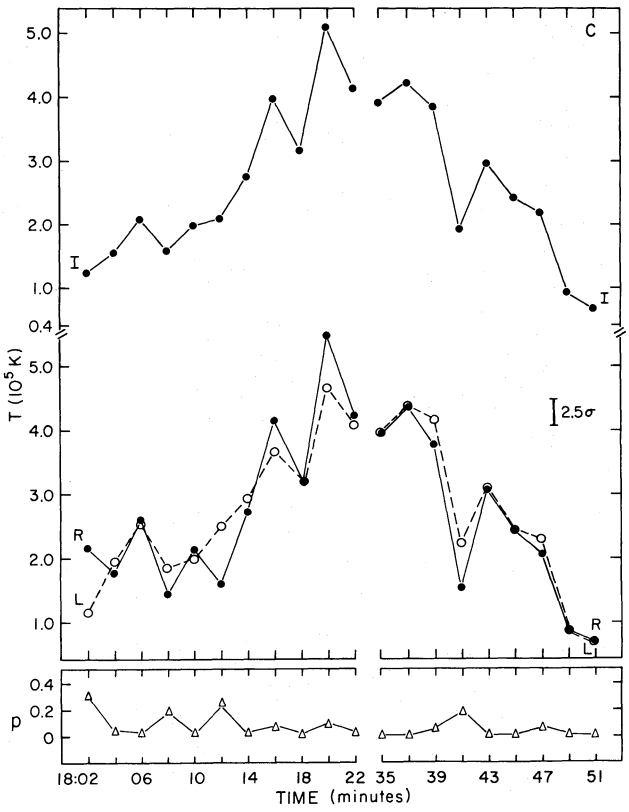

FIG. 6.—Same as Fig. 4 for source C

© American Astronomical Society • Provided by the NASA Astrophysics Data System

1986ApJ...306..740H

Rewriting equation (10) in the form

$$a_x = \frac{T_x}{T_{\max} - T_x} \tag{11a}$$

and

$$a_o = \frac{T_o}{T_{\max} - T_o} \tag{11b}$$

enables one to compute a_x and a_o as a function of time using the observed quantities T_x and T_o, with the coronal temperature, $T_{\max}$, as the only free parameter. Subsequently, when $T_x \neq T_o$, $B|\cos\alpha|$ can be deduced from the ratio a_x/a_o using equation (8), and P_0^2/F_c can also be computed. The case $T_x = T_o$ implies that $B|\cos\alpha|$ is negligible. In that case, no estimate of $B|\cos\alpha|$ can be made, but the ratio P_0^2/F_c can still be computed using equation (8) by neglecting the term $B|\cos\alpha|$, i.e.,

$$\frac{P_0^2}{F_c} = \frac{a_x \omega^2}{7.7 \times 10^{-6}} . \tag{12}$$

Choosing $T_{\max} = 1.5 \times 10^6$ K, as the quiet-Sun coronal temperature, we show, in Figure 7, P_0^2/F_c and $B|\cos\alpha|$, as derived from the observed brightness temperature T_x and T_o of sources A, B, and C as a function of time. (Although the "true" brightness temperature is more likely to be the observed brightness temperature with the background of 5×10^4 K added to it (G. Hurford, private communication), the background was not included in the computations leading to the results shown in Figure 7. Its inclusion would increase the ratio P_0^2/F_c by an average of 25% and decrease $B|\cos\alpha|$ by a comparable factor; the overall variation in time in both quantities, however, remains unchanged). We note from these results that the observed changes in time of the total brightness temperature reflect changes in both P_0^2/F_c and $B|\cos\alpha|$. The latter quantity represents the minimum magnetic field strength, since we cannot independently derive a value for α. We find that the minimum field strength varies between 50 and 200 G, with an average of $\sim$60 G for these three sources. We also find that P_0^2/F_c averages $\sim 2 \times 10^{24}$, which is consistent with quiet-Sun values deduced from EUV measurements (Withbroe and Noyes 1977). The P_0^2/F_c values vary slightly with the assumed coronal temperature $T_{\max}$, while $B|\cos\alpha|$ is barely sensitive to the choice of $T_{\max}$, as would be expected.

IV. DISCUSSION

The observed temporal variations in the radio brightness temperature of the coronal bright points appear to be caused primarily by changes in the pressure P_0 or conductive flux F_c,

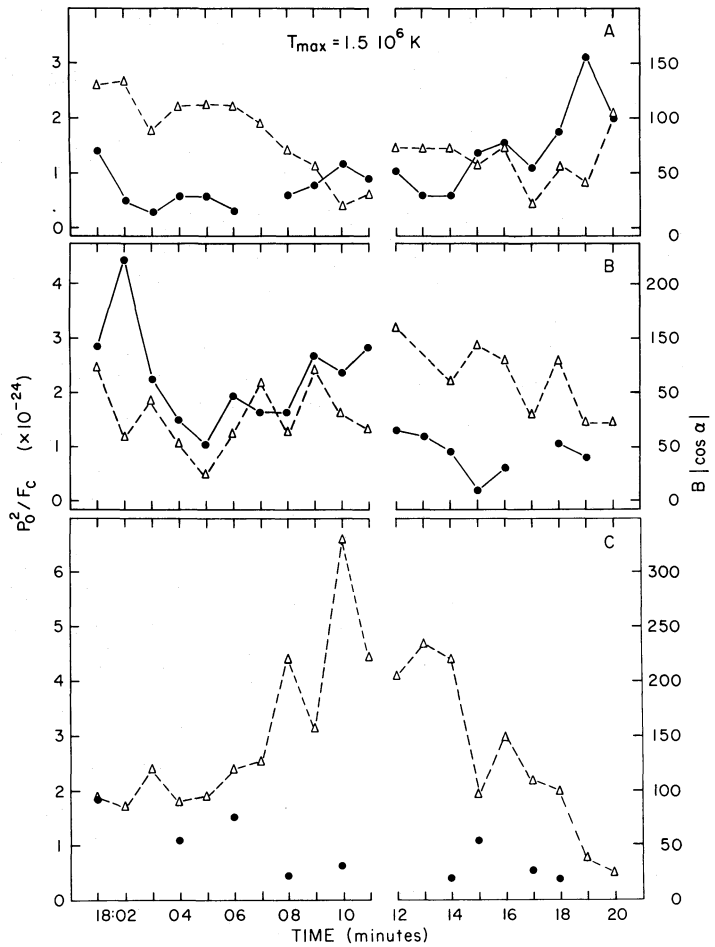

FIG. 7.—The ratio P_0^2/F_c (*open triangles, dashed line*) and $B|\cos\alpha|$ (*filled circles, solid line*) as a function of time as deduced from the observed brightness temperature of the right and left circularly polarized waves in the three bright points A, B, and C, for an assumed coronal temperature $T_{\max} = 1.5 \times 10^6$ K. Values for $B|\cos\alpha|$ are absent when $T_x = T_o$.

© American Astronomical Society • Provided by the NASA Astrophysics Data System

1986ApJ...306..740H

or both. The most likely explanation for these changes are changes in the plasma heating. EUV observations of quiet regions and solar activity indicate that variations in the ratio P_0^2/F_c are strongly correlated with the amount of plasma heating in the upper chromosphere, chromospheric-coronal transition region and corona (see review by Withbroe 1981 and references therein). For example, when the coronal heating rate increases, both the pressure and conductive flux increase in order to balance the increased amount of heating by increased radiative output and larger conductive flux to the chromosphere. Since the temporal variations do not follow any seemingly uniform pattern, the heating process in the observed features is very likely to be chaotic. The observed fluctuations in $B|\cos\alpha|$ would be consistent with an active participation of the magnetic field in the heating process. In either case the deduced magnetic field fluctuations are real and should be kept in mind in any attempt to interpret the observations.

So far we have based our analysis and discussion on the assumption that the radio emission is free-free. The other possible mechanism would be emission due to the gyroresonance of electrons. In the case of gyroresonance absorption the optical depth of the two wave modes is very different (see Zheleznyakov 1970) unless the angle α between the magnetic field direction and the line of sight is very large. Since the observed degree of polarization, which reflects the difference between the brightness temperature of the two wave modes, is rather small ($<40\%$; see Figs. 4–6), gyroresonance absorption can be invoked only if the angle α is large ($>60°$). The observed emission most likely originated in the transition region in magnetic loops where the field lines were probably close to radial. Hence, although it is unlikely that the gyroresonance mechanism was responsible for the observed emission, this mechanism cannot be totally ruled out. The analysis given above is based on the assumption of free-free emission, it yields plasma parameters consistent with observations at other wavelengths.

V. CONCLUSION

This paper reports on the detection of solar coronal bright points at the radio wavelength of 20 cm. The observations were made with the VLA in the B-configuration when the best spatial resolution is 4″. However, the choice of a beam size of 15″ for the CLEANing process has degraded this resolution to 15″. The sources were found to have a spatial extent of ~40″ and the brightness temperature observed ranged from 5×10^4 K to 5×10^5 K, temperatures typical of the transition region. We find that on a time scale of a few minutes the bright points exhibit significant temporal and spatial changes in their brightness temperature, although not always correlated.

Analysis of the data, based on the assumption of free-free emission, reveals that the temporal fluctuations in brightness temperature are due to fluctuations in the pressure, the conductive flux, and the magnetic field strength, as well as direction. An average pressure $P_o = NT = 2 \times 10^{15}$ cm^{-3} K and an average conductive flux $F_c \approx 2 \times 10^6$ ergs cm^{-2} s^{-1}, which are consistent with EUV measurements of bright points (Habbal and Withbroe 1981), yield the average observed ratio $P_0^2/F_c = 2 \times 10^{24}$ K^{2}s ergs^{-1} cm^{-4}. The observed temporal fluctuations of the ratio P_0^2/F_c are signatures of heating. The minimum magnetic field strength deduced from the observation of the brightness temperature of the two wave modes fluctuates between 50 and 200 G. Since the observations made by Harvey (1985) suggest that some bright points are often due to encounters of flux of opposite polarity, the fluctuations in the magnetic field strength and direction inferred from our data could be manifestations of this effect. However, since the structure of the underlying magnetic field is not resolved with the present set of data, we cannot determine whether the magnetic field is playing an active role, as suggested by Parker (1975), or a passive role, in the observed temporal and spatial behavior of the bright points.

We thank Jack Harvey for providing us with the magnetogram and He λ10830 spectroheliogram of 1984 February 11 and for providing, prior to the acquisition of the radio observations, the location of bright points and coronal holes on a He λ10830 spectroheliogram of the Sun taken on 1984 February 9. We also wish to thank G. Hurford and D. Gary for very stimulating discussions, and M. Reid for very useful suggestions on the acquisition and analysis of radio data. This work was supported by funding from the Smithsonian Institution and by NASA grant NAGW-249. The work of the University of Maryland was supported by NSF grant ATM 84-15388 and NASA grant NGR 21-002-199.

REFERENCES

Clark, B. G. 1980, *Astr. Ap.*, **89**, 377.
Dulk, G. A. 1985, *Ann. Rev. Astr. Ap.*, **23**, 169.
Dulk, G. A., and Gary, D. E. 1983, *Astr. Ap.*, **124**, 103.
Golub, L., Krieger, A. S., Vaiana, G. S., Silk, J. K., and Timothy, A. F., 1974, *Ap. J.* (*Letters*), **189**, L93.
Habbal, S. R., and Withbroe, G. L. 1981, *Solar Phys.*, **69**, 77.
Harvey, K. 1985, *Australian J. Phys.*, **38**, 875.
Kundu, M. R. 1965, *Solar Radio Astronomy* (New York: Interscience).
Kundu, M. R., Gergely, T. E., and Golub, L. 1980, *Ap. J.* (*Letters*), **236**, L87.
Marsh, K. A., and Hurford, G. J. 1982, *Ann. Rev. Astr. Ap.*, **20**, 497.
Marsh, K. A., Hurford, G. J., and Zirin, H. 1980, *Ap. J.*, **236**, 1017.
Parker, E. N. 1975, *Ap. J.*, **201**, 494.
Sheeley, N. R., Jr., and Golub, L. 1979, *Solar Phys.*, **63**, 119.
Withbroe, G. L., 1981, in *Solar Active Regions*, ed. F. Q. Orrall (Boulder: Colorado Associated University Press), p. 199.
Withbroe, G. L., and Noyes, R. G. 1977, *Ann. Rev. Astr. Ap.*, **15**, 363.
Zheleznyakov, V. V. 1970, *Radio Emission of the Sun and Planets* (New York: Pergamon Press).

SHADIA R. HABBAL, ROBERT S. RONAN, and GEORGE L. WITHBROE: Harvard Smithsonian Center for Astrophysics, 60 Garden Street, Cambridge MA 02138

MUKUL R. KUNDU: Astronomy Program, University of Maryland, College Park, MD 20742

RAGHUNATH K. SHEVGAONKAR: Indian Institute of Astrophysics, Bangalore 560034, India

© American Astronomical Society • Provided by the NASA Astrophysics Data System